UC Berkeley
UC Berkeley Previously Published Works

Title
High-throughput patterning of photonic structures with tunable periodicity

Permalink
https://escholarship.org/uc/item/14t703rq

Journal
Proceedings of the National Academy of Sciences of the United States of America, 112(17)

ISSN
0027-8424

Authors
Kempa, Thomas J
Bediako, D Kwabena
Kim, Sun-Kyung
et al.

Publication Date
2015-04-28

DOI
10.1073/pnas.1504280112

Peer reviewed

eScholarship.org Powered by the California Digital Library
University of California

CrossMark

High-throughput patterning of photonic structures with tunable periodicity

Thomas J. Kempa[a,1,2], D. Kwabena Bediako[a,1], Sun-Kyung Kim[b,1], Hong-Gyu Park[c,2], and Daniel G. Nocera[a,2]

[a]Department of Chemistry and Chemical Biology, Harvard University, Cambridge, MA 02138; [b]Department of Applied Physics, Kyung Hee University, Gyeonggi-do 446-701, Republic of Korea; and [c]Department of Physics, Korea University, Seoul 136-701, Republic of Korea

Contributed by Daniel G. Nocera, March 12, 2015 (sent for review December 2, 2014)

A patterning method termed "RIPPLE" (reactive interface patterning promoted by lithographic electrochemistry) is applied to the fabrication of arrays of dielectric and metallic optical elements. This method uses cyclic voltammetry to impart patterns onto the working electrode of a standard three-electrode electrochemical setup. Using this technique and a template stripping process, periodic arrays of Ag circular Bragg gratings are patterned in a high-throughput fashion over large substrate areas. By varying the scan rate of the cyclically applied voltage ramps, the periodicity of the gratings can be tuned in situ over micrometer and submicrometer length scales. Characterization of the periodic arrays of periodic gratings identified point-like and annular scattering modes at different planes above the structured surface. Facile, reliable, and rapid patterning techniques like RIPPLE may enable the high-throughput and low-cost fabrication of photonic elements and metasurfaces for energy conversion and sensing applications.

nanopattern | electrochemistry | photonics | silicon | nanofabrication

Developments in photonics and plasmonics have provided a rich array of approaches for coupling and guiding light (1–5) in optoelectronic and energy applications. The structured surfaces required for photon management would ideally feature: (*i*) submicrometer to nanoscale feature size, (*ii*) precise control of feature size and periodicity over a broad range of length scales, (*iii*) structures that can be formed over reasonably large substrate areas, and (*iv*) the capacity to integrate metal and dielectric structures with various substrate geometries. To date, the fabrication of nanoscale and submicrometer structures has relied on a rich repertoire of patterning and assembly techniques (6–15). Aside from well-established techniques such as photolithography, electron-beam lithography, and focused ion beam (6), more recent patterning and assembly methods include directed and self-assembly (7–9), superlattice nanowire pattern transfer (10), dip-pen lithography (11–13), soft-lithography (14), and electrochemical lithography (15). Among these strategies there are the expected trade-offs between fidelity and resolution. In addition, patterning speed, scalability, and the cost/ease of implementation are important factors affecting the feasibility of a given method toward preparing structured surfaces for optical management.

Reactive interface patterning promoted by lithographic electrochemistry (RIPPLE) is a method to form and propagate periodically spaced submicrometer structures over large areas. We demonstrate the ability of the method to pattern optical elements with facility while maintaining control over fidelity and resolution to allow for the fabrication of arrays of dielectric and metallic optical elements. Photonic elements consisting of Ag circular Bragg gratings and large-area periodic arrays of these periodically structured elements were prepared and characterized. The ability to pattern complex submicrometer structures over large areas in a facile, reliable, and timely manner has significant implications for fabrication of photonic elements and metasurfaces (16, 17) for energy and sensing applications.

Results and Discussion

The RIPPLE method can rapidly pattern large areas of a substrate with periodic nanoscale features composed of oxidic or metallic species. This method uses cyclic voltammetry to impart patterns onto the working electrode of a standard three-electrode electrochemical setup (Fig. 1*A*). A parent material, which can be a semiconductor (e.g., Ge) or metal (e.g., Cu), is deposited by chemical or physical vapor deposition over the working electrode. Subsequently, a thin layer of polymer resist is dispersed over this parent layer and defined with lines or dots, which give the electrolyte access to the underlying parent film. The substrate thus prepared is the working electrode in a standard two-compartment electrochemical cell filled with 0.1 M sulfuric acid as the electrolyte. Details of the substrate preparation and cyclic voltammetry are provided in *Materials and Methods*. By applying a linearly ramped potential sweep (0.1–1.2 V; all potentials are referenced to the Ag/AgCl electrode) between the working electrode and a Pt mesh counterelectrode, we promote etching of the parent material, which originates at the site of the lines/dots exposed to solution and then propagates underneath the resist.

To demonstrate the capabilities of the RIPPLE technique, a Ge thin film was deposited over a Si substrate and the overlaid polymer photolithographically defined with an array of 2-μm-wide lines (*Materials and Methods*). After applying the cyclic voltammetric potential sweeps to this working electrode and subsequent stripping of the resist, an atomic force microscopy (AFM) map of a region of one pattern reveals well-defined

Significance

Patterning large substrate areas with arrays of submicrometer structures in a facile, reliable, and timely manner is important for fabrication of optical elements that capture, guide, and convert light. RIPPLE (reactive interface patterning promoted by lithographic electrochemistry) is an electrochemical patterning method that is demonstrated for the rapid fabrication of periodic arrays of metallic circular Bragg gratings over large substrate areas. The grating period can be tuned in situ over micrometer and submicrometer length scales in a high-throughput fashion. We have identified point-like and annular scattering modes at different planes above the structured surface, suggesting the potential to use such structures to control the propagation of light. The described methods may be useful for high-throughput fabrication of sensors and light-management elements for energy conversion applications.

Author contributions: T.J.K., D.K.B., and D.G.N. designed research; T.J.K., D.K.B., and S.-K.K. performed research; T.J.K. contributed new reagents/analytic tools; T.J.K., D.K.B., H.-G.P., and D.G.N. analyzed data; and T.J.K. and D.G.N. wrote the paper.

The authors declare no conflict of interest.

[1]T.J.K., D.K.B., and S.-K.K. contributed equally to this work.

[2]To whom correspondence may be addressed. Email: tkempa@fas.harvard.edu, hgpark@korea.ac.kr, or dnocera@fas.harvard.edu.

This article contains supporting information online at www.pnas.org/lookup/suppl/doi:10.1073/pnas.1504280112/-/DCSupplemental.

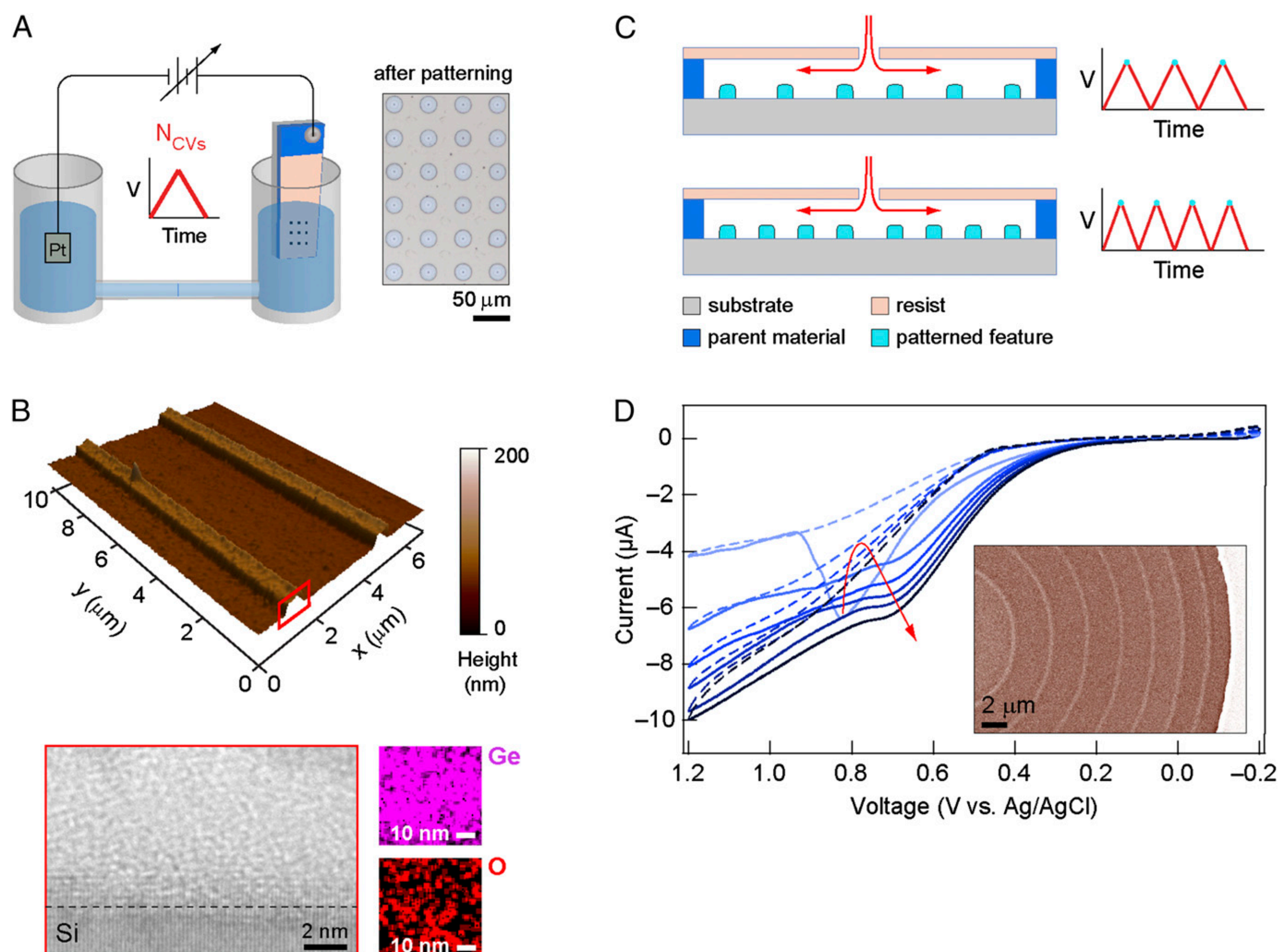

Fig. 1. (*A*) Schematic of the RIPPLE process. (*Left*) A standard three-electrode electrochemical setup is used. A working electrode is covered with the parent material (dark blue) to be patterned. Lastly, a top layer of resist (pink) is deposited and prepared with micrometer-scale dots or lines, which give the electrolyte access to the parent material. A series of cyclic voltammetric sweeps (N_{CVs}) are performed in acidic electrolyte to periodically pattern the working electrode. (*Right*) Periodic arrays of periodic circular structures are formed rapidly as shown in the optical image. The area beyond the circles is the unpatterned parent film covered by resist. (*B*, *Top*) AFM topographical map of two linear features patterned using the RIPPLE process. (*Bottom*) Bright-field TEM image of the axial cross-section of a representative feature as noted with the red box. Dashed line denotes the interface between underlying Si substrate and the deposited feature. EDS maps of Ge and O sampled from within the feature region (light contrast) in the TEM image at left. (*C*) During cyclic application of voltage ramps, lateral etching of the parent material occurs in concert with site-specific localization of nanoscale periodic features (light blue). The number of features is controlled by the number of CVs whereas their period is controlled by voltage scan rate. (*D*) CV data for a patterning experiment lasting eight cycles (for clarity, only cycles 1, 3, 4, 5, 7, and 8 are shown). Solid line, anodic sweep; dashed line, cathodic sweep. Red line is intended as a guide for the eye showing peak evolution from cycle 1–8. (*Inset*) SEM image of a portion of the concentric rings patterned from a single dot at a scan rate of 100 mV/s.

parallel lines of submicrometer width and height (Fig. 1*B*, *Top*). Over the range of cyclic voltammogram (CV) scan rates used in patterning (50 to 200 mV/s), the features are 20(±1) nm high and 360(±15) nm wide. Transmission electron microscopy (TEM) cross-sections reveal the features to have an amorphous morphology whereas energy dispersive X-ray spectroscopy (EDS) maps show them to be composed of Ge and O (Fig. 1*B*, *Bottom*). A feature composed of an oxide of germanium is consistent with the thermodynamically favored products of oxidation of Ge at pH 1 and applied potentials used for patterning. Aside from linear features, concentric rings can be patterned easily from dots defined through the resist layer to the underlying parent material. Cyclic application of voltage ramps leads to lateral etching of the parent material as well as site-specific localization of nanoscale periodic features, the number of which is defined by $N_{CV} - 1$, where N_{CV} is the number of CV scans (Fig. 1*C*). In particular, we found that the period separating features shows a power-law dependence on CV scan rate and are able to finely control this spacing from 500 nm to 10 μm (*SI Appendix*, Fig. S1). We note from an examination of CV sweeps and SEM and TEM images (*SI Appendix*, Fig. S1) that patterning occurs by complete etching of the Ge film to expose the underlying Si substrate and localization at the interface between the periphery of the unetched Ge film and exposed Si substrate. The lateral extent of etching is controlled by CV and electrolyte conditions, which provide the driving force and pH required for formation of the aqueous species of the parent material as predicted by its Pourbaix phase diagram. The localization of oxidic Ge ridge pattern (rings and lines) forms at the point where the CV scan direction changes from anodic to cathodic sweep. The patterns appear similar to those generated from moving boundary simulations of etching processes (18). Though pattern formation appears electrochemically mediated, capillary flows leading to contact line pinning and depinning (19) at the periphery of the unetched parent material may intervene in the generation of periodic features.

The versatility and structural control afforded by the RIPPLE method was exploited to fabricate large-area arrays of photonic elements. A resist layer coating a 250-nm film of Ge (parent material) was photolithographically patterned with a 0.25-mm^2 square array of 2 × 2-μm dots separated by 60 μm. A typical patterning experiment lasting eight CV cycles performed between –0.2 and 1.2 V (vs. Ag/AgCl) at 100 mV/s on the aforementioned substrate (working electrode) is shown in Fig. 1*D* (*Materials and Methods*). The anodic sweep on the first CV cycle is characterized by a large peak at 0.8 V and subsequent CV cycles show a well-conserved broad peak near this potential. The amplitude of this broad feature is initially smaller than that of the dominant peak of the first CV sweep, but monotonically increases for subsequent cycles. Cathodic sweeps are consistently featureless compared with anodic sweeps. Emanating from the site of each predefined dot in the array is a structure consisting of seven concentric periodically spaced rings. AFM analysis of a portion of one structure reveals a feature height, width, and period of 20 nm, 360 nm, and 2.7 μm, respectively (Fig. 1*D*, *Inset*). The large peak of the first anodic sweep arises from the large mass of Ge that undergoes oxidation to form the etched region at the center of each concentric ring structure. The predefined dot size defines the diameter of this initial etched region before localization of the first ring. Thereafter, the spacing between rings is dictated by the scan rate and the voltage range swept out during CV cycles. The monotonic increase of the broad peak occurs in concert with expansion of the etched region between periodically deposited rings. The dispersion in period and feature size is <3% and <5%, respectively. We have patterned features with diameters as large as 80 μm. We surmise that the lateral etching limit is defined by the resist's elastic modulus, which, if exceeded, would cause the resist to collapse, thereby restricting the electrolyte filled space.

Periodic circular or linear patterns of nonmetallic and metallic submicrometer structures are of interest as waveguides and plasmonic cavities for sensing and integrated optical applications (20, 21). The features patterned by RIPPLE are characterized by low surface roughness, high patterning selectivity, and small dispersion for periods <1 μm, characteristics that are relevant to the design of high-quality optical gratings. We fabricated a Ag circular Bragg grating (CBG) array by template stripping (22) from a periodic array of Ge concentric ring structures (Fig. 2). The Ge concentric ring master pattern (Fig. 2*A*) was prepared using RIPPLE performed over six CV cycles at a voltage scan rate of 290 mV/s to yield structures containing five concentric Ge rings separated by a period of 1 μm. A silver film deposited over the Ge master pattern was subsequently peeled off to reveal an array of CBGs recessed in the film (Fig. 2 *A* and *B*). SEM images confirm that large periodic arrays of intact CBGs, each bearing five grooves separated by a period of 1 μm, can be templated from the master Ge substrate (Fig. 2*C*). An AFM profile composed of the average of 14 linescans acquired across an ∼10 $μm^2$ area of a CBG shows an average groove depth of 15 nm, width of 230 nm, and period of 1 μm (Fig. 2*D*). These dimensions verify that the metallic CBG pattern is a reasonable replica of the Ge master pattern. Notably, the master can be reused multiple times to template other CBG arrays composed of different metals.

To demonstrate the quality of the CBGs, we acquired their scattering profiles. A sample area that consists of nine CBGs in a square array (Fig. 3 *A, 1*) was irradiated with the 500-nm monochromated output of a supercontinuum laser. Images of scattering profiles (Fig. 3 *A*, *2* and *3*) were acquired at two

Fig. 2. (*A*, *Left*) Schematic of a master pattern consisting of a periodic array of periodic concentric rings composed of oxidic Ge. (*A*, *Right*) Schematic of a Ag CBG array templated from the master pattern. (*B*) Schematic of the Ag CBG array fabrication by template stripping. (*C*, *Left*) SEM image of a portion of the Ag CBG array containing 63 intact CBGs. (*Right*, *Top*) SEM image of a single CBG. (*Right*, *Bottom*) SEM image of the periphery of a CBG showing grooves. (*D*) AFM line-scan across a CBG verifying that the depth, width, and period of the grooves are similar to the dimensions of the Ge rings in the master pattern.

slightly different imaging planes within ∼1 μm of the focal plane. These images show that point (Fig. 3 *A*, *2*) and annular (Fig. 3 *A*, *3*) scattering arises from each CBG. In particular, complex "checkerboard" interference patterns are clearly discernible at the interstices between CBGs (Fig. 3 *A*, *3*). Such structured scattering is unique to a periodic array of periodic grating structures, where such surfaces may be interesting candidates for metasurface applications (16, 17) especially given the ease, scale, and configurability with which RIPPLE can pattern them.

To define the origin of the measured scattering modes, we performed finite-difference time-domain (FDTD) simulations of Ag CBGs. A simulated reflectance spectrum for a single CBG having the same dimensions as the patterned structures (Fig. 3*B*) reveals wavelength-dependent variations in reflected amplitude. Of particular interest is a distinct dip in reflectance observed at 505 nm. A simulated near-field *x–y* plane scattering profile at this wavelength acquired at a height of 0.5 μm from the top surface of the CBG (Fig. 3*B*, *Inset*) reveals point scatter from the center of the CBG as well as more complex annular scatter from its periphery. A simulation (axial view) of the electric fields normal to the Ag–air interface of the CBG at 505 nm shows that these fields propagate with alternating phase along this interface (Fig. 3*C*). This result is diagnostic of the presence of surface plasmon polaritons, which are excited by interaction of the incident plane wave with the periodic grooves of the CBG (23, 24). Together, simulation and theory not only reconstitute the essential features of the scatter profiles measured in Fig. 3*A*, but also suggest a role for surface plasmon polaritons in the spatial control of scattering from these Ag CBGs.

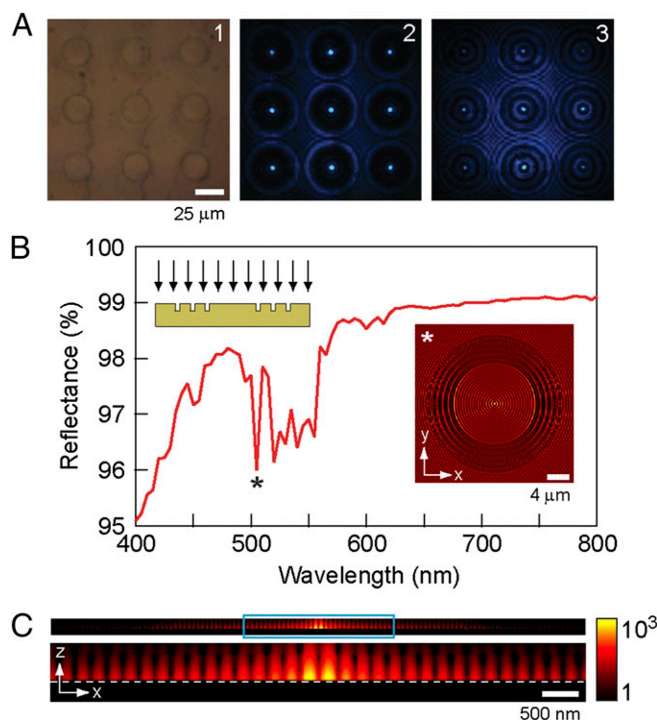

Fig. 3. (*A*, *1*) CCD image of nine CBGs arranged into a square array. (*A*, *2* and *3*) CCD images of the scattering profiles detected above the CBG array surface for 500-nm plane-wave illumination. (*B*) Simulated reflectance spectrum for a CBG having equivalent dimensions to the fabricated and measured one in Fig. 2*C*. The asterisk denotes the dip in reflectance at 505 nm. (*Inset*) Simulated near-field scattering profile of a CBG obtained by acquiring the projection of the Poynting vector on a plane (*x–y*) 0.5 μm above the CBG surface. (*C*, *Top*) Axial view (*x–z* plane) of the electric field intensity, plotted as log(E^2), normal to the Ag–air interface of the CBG for 505-nm plane-wave illumination. (*C*, *Bottom*) Magnified view of the cross-section bounded by the teal box above. Dashed white line denotes Ag–air interface.

Conclusion

We have shown that through a combination of the RIPPLE technique and template stripping, periodic arrays of periodic optical elements can be easily and rapidly patterned over large areas of a substrate. Detection of point-like and annular scattering modes attests to the fidelity of the patterns and their potential to control the spatial profile of light emanating from them. A number of promising studies and technologies related to photonics (25, 26), plasmonics (1–5), and metasurfaces (16, 17) are contingent on the ability to pattern nanoscale to submicrometer features that are periodic over large areas, with large-area patterning being the key challenge. To this end, we view RIPPLE as providing some compelling attributes, including the ability (*i*) to control pattern periodicity in situ, with CV scan rate, from <1 μm to several tens of μm, (*ii*) to pattern rapidly over large substrate areas, and (*iii*) to pattern easily using low-cost and generic chemicals and equipment.

We also note that direct patterning of metallic and dielectric gratings is possible, thus obviating the need for a template stripping process. Furthermore, it may be possible to operate RIPPLE in a purely additive mode wherein periodic deposition takes place from solution-phase precursors delivered via microfluidic arrays. High-quality optical elements characterized by low surface roughness, sharp pattern profiles, and a small dispersion in submicrometer periods are required to fully capitalize on the promise of RIPPLE as a fabrication technique for optical applications. With a detailed understanding of the patterning mechanism and materials limits, further insights into key parameters dictating resolution and quality will emerge. For example, by tailoring the surface tension and viscosity of the electrolyte solution, we anticipate being able to reduce the size of patterned features, to increase the steepness of feature sidewalls, and to reduce surface roughness. In general, our findings establish the viability of implementing RIPPLE-based structures in photonics and plasmonics, where high-throughput and reliable methods are needed to pattern dielectric and metallic elements over large areas.

Materials and Methods

RIPPLE Fabrication. Silicon p-type doped substrates (Prime Grade 3–5 Ω cm, Nova Electronic Materials) of dimension 2 cm^2 were cleaned by UV/ozone ashing followed by etching in buffered hydrogen fluoride. A home-built chemical vapor deposition reactor was used to grow a 250-nm-thick polycrystalline p-type Ge film at 330 °C at a growth pressure of 28 torr. After Ge deposition, the substrate was coated with a 500-nm-thick layer of S1805 photoresist (S1805, MicroChem Corp.) or poly(methyl methacrylate) (PMMA) e-beam resist (PMMA C5, MicroChem Corp.). Using photolithography or electron beam lithography, 2 μm × 2-μm dots were defined through the aforementioned resists to the underlying Ge film. A portion of the substrate was left free of resist to facilitate electrical contact of this working electrode via a Cu alligator clip to the potentiostat. The back and sides of the substrate were covered with a lacquer (Microshield, Tolber Chemical) to prevent electrolyte exposure to these regions. A two-compartment electrochemical cell was filled with 0.1 M sulfuric acid. The substrate (working electrode) was submerged into one compartment. *i*R compensation was performed before every patterning experiment and yielded typical resistance values in the range of 500–1,500 Ω. Standard three-electrode cyclic voltammetry experiments were conducted using a Ag/AgCl reference electrode (BAS Inc.), a Pt mesh counterelectrode, and potentiostat (760D series, CH Instruments Inc.). Following cyclic voltammetry, all resists and lacquer were removed by soaking the substrate in acetone for ∼1 min followed by a 10-s rinse in isopropanol. A gentle stream of N_2 enabled drying. For Ge patterning, scans were initiated at the open circuit potential, which was 0.1 V.

Preparation of CBG. A 0.25-mm^2 square array containing 81 concentric ring structures was patterned using RIPPLE. Each structure had five Ge rings with a period of 1 μm patterned via six CV cycles at a voltage scan rate of 290 mV/s. A 150-nm Ag film was deposited over this Ge master pattern by electron-beam

evaporation (Denton Vacuum LLC) after pumping to a base pressure of 2×10^{-7} torr. Next the Ag film side of the sample was pressed into contact with a clean quartz slide coated with a thin film of epoxy. The sample was cured overnight. After this, the Ge master pattern was peeled away from the Ag film using tweezers. The resultant Ag film remained fused to the quartz substrate and bore a high yield of recessed concentric ring structures. These recessed structures constitute the array of CBGs, which were analyzed in Fig. 3.

Acquisition of Scattering Profiles. To obtain scattering profiles from a CBG prepared by RIPPLE, a broadband (λ = 450–800 nm) supercontinuum laser (EXB-6, NKT Photonics) was used as an illumination source. A spectrometer (SpectraPro 300i, Acton Research) was used to select a narrowband illumination with a central wavelength of $\lambda = 500$ nm. The scattering images were captured by a Si charge-coupled device whereas the CBG specimen was translated through the focal plane of a 10× optical lens.

FDTD Simulations. FDTD simulations were used to calculate the near- and far-field scattering profiles from a CBG. A nonuniform grid method was used to accurately model light propagation in our experiment. To this end, we used a spatial resolution of 1 nm at the metal–dielectric interface and 5 nm elsewhere in the simulation domain. The dispersive optical constants of silicon and silver were obtained by fitting their measured refractive index and extinction coefficient over the wavelength range λ = 400–800 nm. The reflectance spectrum from interaction of a normally incident plane wave with the CBG was acquired from 400 to 800 nm in 5-nm increments. The total-field scattered-field method was applied to ensure that the CBG experiences an infinitely extended plane wave. The near-field profile was calculated by obtaining the normal Poynting vector at a plane 500 nm away from the top surface of a CBG.

ACKNOWLEDGMENTS. D.G.N. acknowledges support of this work by National Science Foundation Center for Chemical Innovation Center CHE-1305124. S.-K.K. acknowledges support of this work by Basic Science Research Program through the National Research Foundation of Korea (NRF) funded by the Ministry of Science, Information/Communication Technology & Future Planning (NRF-2013R1A1A1059423). H.-G.P. acknowledges support by an NRF Grant (2009-0081565) funded by the Korean government (Ministry of Science, Information/Communication Technology, and Future Planning). We thank TomKat Trust for funding of the First 100 Watts Project.

1. Atwater HA, Polman A (2010) Plasmonics for improved photovoltaic devices. *Nat Mater* 9(3):205–213.
2. Ozbay E (2006) Plasmonics: Merging photonics and electronics at nanoscale dimensions. *Science* 311(5758):189–193.
3. Xu T, Agrawal A, Abashin M, Chau KJ, Lezec HJ (2013) All-angle negative refraction and active flat lensing of ultraviolet light. *Nature* 497(7450):470–474.
4. Jun YC, Huang KCY, Brongersma ML (2011) Plasmonic beaming and active control over fluorescent emission. *Nat Commun* 2(283):283.
5. Laux E, Genet C, Skauli T, Ebbesen TW (2008) Plasmonic photon sorters for spectral and polarimetric imaging. *Nat Photonics* 2:161–164.
6. Madou MJ (2011) Manufacturing techniques for microfabrication and nanotechnology. *Fundamentals of Microfabrication and Nanotechnology* (CRC Press, Boca Raton, FL), 3rd Ed, Vol II.
7. Xia Y, Gates B, Yin Y, Lu Y (2000) Monodispersed colloidal spheres: Old materials with new applications. *Adv Mater* 12(10):693–713.
8. Jeong S, et al. (2010) Fast and scalable printing of large area monolayer nanoparticles for nanotexturing applications. *Nano Lett* 10(8):2989–2994.
9. Pinheiro AV, Han D, Shih WM, Yan H (2011) Challenges and opportunities for structural DNA nanotechnology. *Nat Nanotechnol* 6(12):763–772.
10. Heath JR (2008) Superlattice nanowire pattern transfer (SNAP). *Acc Chem Res* 41(12):1609–1617.
11. Piner RD, Zhu J, Xu F, Hong S, Mirkin CA (1999) "Dip-Pen" nanolithography. *Science* 283(5402):661–663.
12. Huo F, et al. (2008) Polymer pen lithography. *Science* 321(5896):1658–1660.
13. Huo F, et al. (2010) Beam pen lithography. *Nat Nanotechnol* 5(9):637–640.
14. Love JC, Estroff LA, Kriebel JK, Nuzzo RG, Whitesides GM (2005) Self-assembled monolayers of thiolates on metals as a form of nanotechnology. *Chem Rev* 105(4):1103–1169.
15. Simeone FC, Albonetti C, Cavallini M (2009) Progress in micro- and nanopatterning via electrochemical lithography. *J Phys Chem C* 113(44):18987–18994.
16. Kildishev AV, Boltasseva A, Shalaev VM (2013) Planar photonics with metasurfaces. *Science* 339(6125):1232009.
17. Lin D, Fan P, Hasman E, Brongersma ML (2014) Dielectric gradient metasurface optical elements. *Science* 345(6194):298–302.
18. West AC, Madore C, Matlosz M, Landolt D (1992) Shape changes during through-mask electrochemical micromachining of thin-metal films. *J Electrochem Soc* 139(2):499–506.
19. Deegan RD, et al. (1997) Capillary flow as the cause of ring stains from dried liquid drops. *Nature* 389:827–829.
20. Delacour C, et al. (2010) Efficient directional coupling between silicon and copper plasmonic nanoslot waveguides: Toward metal-oxide-silicon nanophotonics. *Nano Lett* 10(8):2922–2926.
21. Sugawa K, et al. (2013) Metal-enhanced fluorescence platforms based on plasmonic ordered copper arrays: Wavelength dependence of quenching and enhancement effects. *ACS Nano* 7(11):9997–10010.
22. Nagpal P, Lindquist NC, Oh SH, Norris DJ (2009) Ultrasmooth patterned metals for plasmonics and metamaterials. *Science* 325(5940):594–597.
23. Barnes WL, Dereux A, Ebbesen TW (2003) Surface plasmon subwavelength optics. *Nature* 424(6950):824–830.
24. Kim SK, et al. (2011) Surface-plasmon-induced light absorption on a rough silver surface. *Appl Phys Lett* 98(1):011109.
25. Lopez C (2003) Materials aspects of photonic crystals. *Adv Mater* 15(20):1679–1704.
26. Jalali B, Fathpour S (2006) Silicon photonics. *J Lightwave Technol* 24(12):4600–4615.